

3D Map Modeling Using Static Photo Images and Video Images of Environment around a River Captured by a Fisheye-Lens Camera Mounted on a Multi-Rotor Drone

Akhmad Taufik¹, Shingo Okamoto², Jae Hoon Lee³

^{1,2,3} Graduated School of Science and Engineering, Ehime University, Japan

¹ Department of Mechanical Engineering, State Polytechnic of Ujung Pandang, Indonesia

¹ z861004z@mails.cc.ehime-u.ac.jp, ² okamoto.shingo.mh@ehime-u.ac.jp, ³ jhlee@ehime-u.ac.jp

Abstract-- The purposes of this research are to create a 3D textured map by using image processing of static photo images and video images of an environment around a river and a 3D map model of the environment by using a 3D color printer. Firstly, static photo images and video images of the targeted environment around the river were captured by the fisheye-lens camera mounted on a multi-rotor drone flight-controlled manually. Then, the image processing consisting of five main steps to create the 3D textured map were performed using the static photo images and video images. Furthermore, a thickened 3D map was built by using a selected area in the 3D textured map of the static photo images. Finally, the 3D map model of the environment around the river was built by using the thickened 3D map and a 3D color printer.

Index Term-- 3D map modeling, image processing, multi-rotor drone, static photo images, video images.

1 INTRODUCTION

In recent years, the 3D map modeling of environments have become more important for various applications, such as area mapping on archaeology or a disaster, building modeling, road inspection, and city planning. The production of 3D map models is supported by the advance of technologies to process digital data such as, photogrammetric image processing softwares and 3D printing.

In the last decade, a number of studies on 3D mapping of environments have been carried out [1] – [16]. As far as the authors reached, only two papers [1] and [2] are reported on 3D mapping of a river environment. In the two papers, 3D point data of vegetation along the river were obtained using a 3D laser scanner installed on Unmanned Aerial Vehicles (UAVs). Then, the other papers are reported on 3D mapping of ground environments. In most of them reported, photo images of the ground environments were captured using conventional-lens cameras installed on UAVs [3] – [9]. In a few studies of them reported, fisheye-lens cameras installed on UAVs were used to capture photo images of the ground environments [10] – [12]. Then, all of them used photogrammetric image processing softwares to reconstruct the photo images into digital 3D data representing the ground environments. Furthermore, a number of studies on 3D modeling of isolated objects have been carried out [13] – [16]. The 3D models in their reports on digital 3D data were produced by using 3D monochrome printers. However, there is no report in which a 3D map model of an environment around a river was produced using the method proposed by the authors in this paper.

The authors reported on an autonomous flight along a river performed by a multi-rotor drone installing a single-lens camera and image processing [17] - [18]. Then, the method on 3D mapping and 3D modeling using static photo images of an environment around a river captured by the fisheye-lens camera mounted on a multi-rotor drone was introduced by the authors [19]. In this paper, the method on 3D mapping using not only the static photo images but also the video images of the environment around the river was proposed. In the 3D mapping, the video images were extracted from the captured videos. In addition, the 3D maps of the static photo images and video images were compared. Then, the 3D map model was produced by using the data of the better 3D map.

Firstly, the flying experiment to capture the static photo images and the video images of the environment around the river was performed by using a multi-rotor drone with a fisheye-lens camera. Then, the 3D mapping was performed by image processing of the captured static photo images and video images using a photogrammetric image software (Agisoft PhotoScan Professional ver.1.1). Finally, the 3D map model of the environment around the river was produced by using a 3D color printer (IRIS 3D printer).

2 FLYING EXPERIMENT USING A MULTI-ROTOR DRONE WITH A FISHEYE-LENS CAMERA

2.1 Method

Figure 1 shows the multi-rotor drone (Parrot Bebop Drone) with a fisheye-lens camera in the present research. The multi-rotor drone equips with a fisheye-lens camera, a memory card, and a GPS. Static photo images and video images of an environment around a river are captured by the fisheye-lens camera mounted in the front side of the drone and stored in the memory card mounted inside the drone. In addition, 3D coordinates of the drone's positions when capturing the static photo images are measured by the GPS mounted inside the drone.

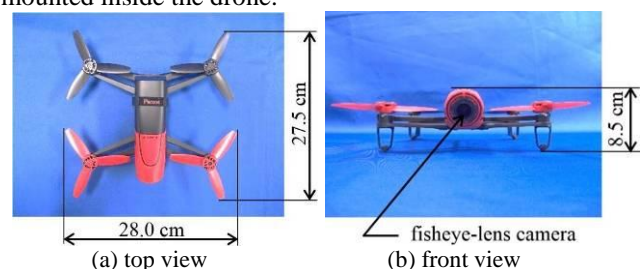


Fig. 1. Multi-rotor drone (Parrot Bebop Drone) with a fisheye-lens camera

Figure 2 shows the environment around a river that is used in this research. The environment is located in a considerable distance from resident's houses, namely around 150 [m]. The environment used in the experiment consists of a curved river with the average width of 5 [m], bush and farmlands at both sides of the river. The static photo images and video images of the environment are captured using a fisheye-lens camera mounted on the multi-rotor drone with a resolution of 14 [Mpx] and a field of view of 180 [°].



Fig. 2. Environment around a river that is used in this research

Figure 3 shows the positions where static photo images and video images of the environment around the river are captured by the fisheye-lens camera mounted on the multi-rotor drone in two straight lines. The drone firstly performed a flight to capture static photo images and video images in the first line. After finishing the flight in the first line, the drone repeated the flight in the second line which parallels to the first one. The 3D coordinates of positions to capture the images were measured by the GPS and saved in the memory card mounted inside the multi-rotor drone.



●: Positions to capture static photo images and video images

Fig. 3. Positions where static photo images and video images were captured by the fisheye-lens camera mounted on the multi-rotor drone

Figure 4 shows the scene in which static photo images and video images of the environment around the river captured by the fisheye-lens camera installed on the Parrot Bebop Drone flight-controlled manually was carried out. The tablet computer to control the drone communicated with the multi-rotor drone through a wireless connection (Wi-Fi). The maximum distance that the Wi-Fi can reach is 150 [m].

Firstly, the multi-rotor drone took off the ground at the river side. Then, the altitude of the multi-rotor drone was increased until 15 [m]. At the altitude, the drone had carried out a hovering for several seconds. After that, the drone had performed the flights to capture the static photo images and video images of the environment around the river in the two straight lines. The static photo images were captured in every 6 [s]. The 3D coordinates of the drone's positions when capturing the static photo images were measured by the GPS. Then, the static photo images with 3D coordinate data were saved in the memory card mounted inside the drone. The video images were captured in 30 [fps]. However, the video images were saved without 3D coordinates of the drone's positions when capturing the video images.



Fig. 4. Scene in which static photo images and videos images of the environment around the river were captured by the fisheye-lens camera installed on the Parrot Bebop Drone flight-controlled manually

2.2 Result

2.2.1 Static Photo Images of an Environment Around a River

Figure 5 shows the examples of overlapping static photo images of the environment around the river captured in every 6 [s] by the fisheye-lens camera mounted on the multi-rotor drone. There are 45 overlapping static photo images captured and saved as JPEG format in the flying experiment. The length and the width of the static photo images are 1,920 [pixels] and 1,088 [pixels], respectively. Each static photo image is overlapping by 80 % with the adjacent photo image.

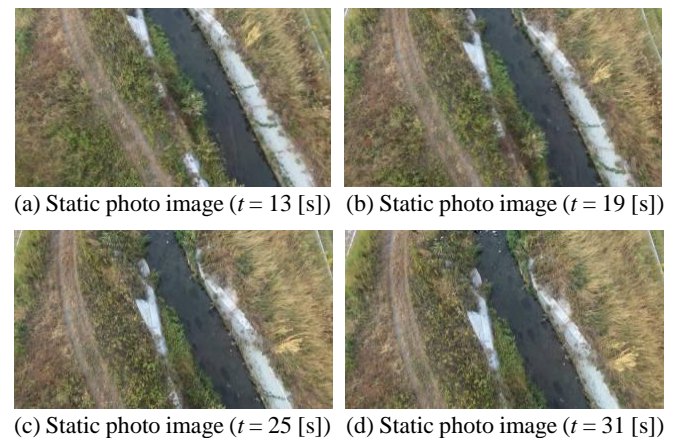


Fig. 5. Examples of overlapping static photo images of the environment around the river captured in every 6 [s] by the fisheye-lens camera mounted on the multi-rotor drone

2.2.2 Video Images of an Environment around a River

Figure 6 shows the examples of overlapping video images of the environment around the river extracted from videos captured by the fisheye-lens camera mounted on the multi-rotor drone. There are 89 overlapping video images extracted from the videos captured in the flying experiment. The length and the width of the video images are 1,920 [pixels] and 1,080 [pixels], respectively.

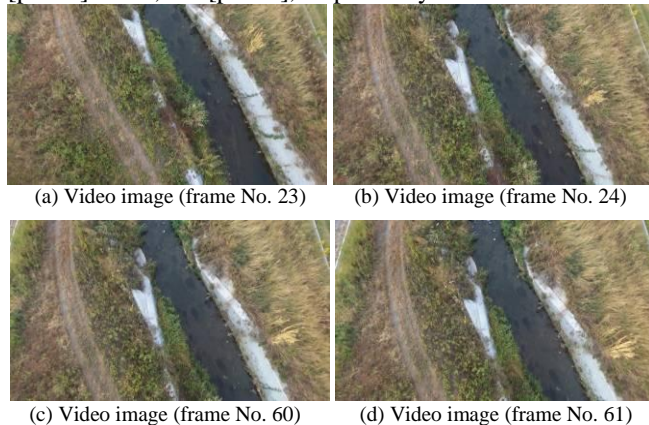


Fig. 6. Examples of overlapping video images extracted from videos of environment around the river captured by the fisheye-lens camera mounted on the multi-rotor drone

3 3D MAPPING USING IMAGE PROCESSING OF STATIC PHOTO IMAGES AND VIDEO IMAGES

In order to build 3D map data of the environment around the river, the captured static photo images and video images were processed using the Agisoft PhotoScan (Ver.1.1). There are five consecutive stages in the 3D mapping, namely the loading and the aligning the images, the building the dense point clouds, the polygonal meshes, and the 3D textured maps as shown in Fig. 7. The image processing were performed using the commands in the workflow menu of the Agisoft.

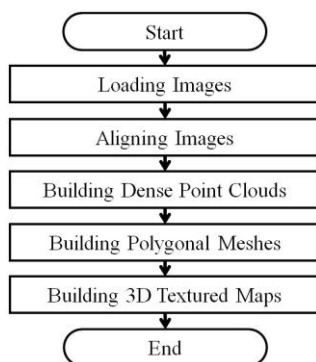


Fig. 7. Five consecutive stages in the 3D mapping to create 3D textured maps using static photo images and video images

3.1 Loading Images

Firstly, two project files of Agisoft PhotoScan were opened to process the static photo images and the video images of the environment around the river. Then, the 45 overlapping static photo images were loaded to the workspace pane in the first project file. The 3D coordinates of the multi-rotor drone's positions when capturing the static photo images measured by the GPS were detected by the Agisoft. After that, the positions were displayed in the model pane based on the 3D coordinate data. Figure 8 shows the positions of the multi-rotor drone when capturing the 45 static photo images displayed in two lines in the model pane

of the Agisoft. Based on those positions, 18 static photo images having no overlapping area with the static photo images in the other line were removed from the workspace pane.

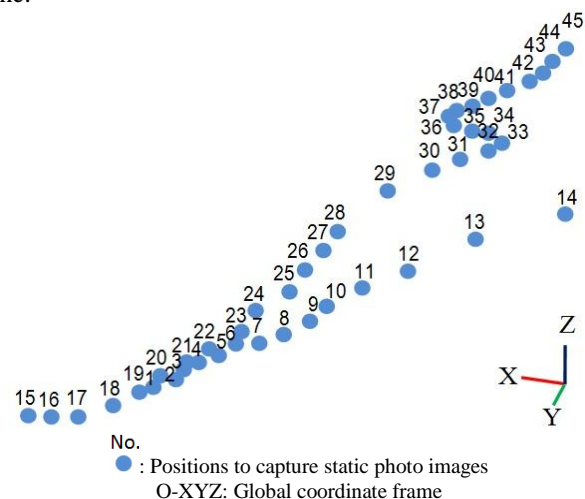


Fig. 8. Positions of the multi-rotor drone when capturing the 45 static photo images displayed in two lines in the model pane of the Agisoft

Furthermore, the 89 overlapping video images of the environment around the river were loaded to the workspace pane in the second project file. However, there was no figure of positions to capture the video images displayed in the model pane due to that the video images do not have 3D coordinates of the positions.

3.2 Aligning Images

In the second process, the point data of static photo images were firstly detected by the Agisoft. Then, the data of each static photo image were compared to their adjacent ones in order to detect matching points between the two static photo images. After that, the matching points and 3D coordinate data were used to estimate the positions and the orientations of static photo images and to build a sparse point cloud. The 7,698 points were generated in the sparse point cloud of the static photo images.

On the other hand, the same process to build a sparse point cloud was performed by the Agisoft using the video images. Due to the absence of 3D coordinate data, only the matching point data of the video images were used to estimate the positions and the orientations of video images and to build a sparse point cloud. The 8,240 points were generated in the sparse point cloud of the video images. Figure 9 shows the estimated positions and orientations of the 27 static photo images and the 89 video images shown by the squares and the sparse point clouds below the positions displayed in the model pane of the Agisoft.

Furthermore, the quality of the 27 static photo images and the 89 video ones were estimated by the Agisoft using the data of the images. The quality of an image is treated by a numerical value in a range from 0.000 to 1.000 where a large value means high quality. The images whose qualities are less than 0.500 are not feasible in using for further processes. Then, the qualities of the static photo images and the video ones were more than 0.500. The average qualities of the static photo images and the video ones were 0.779 and 0.766, respectively. It means that the whole images captured by the fisheye-lens camera were feasible to use them for further processes. Then, the average quality of the static photo images was higher than the video ones.

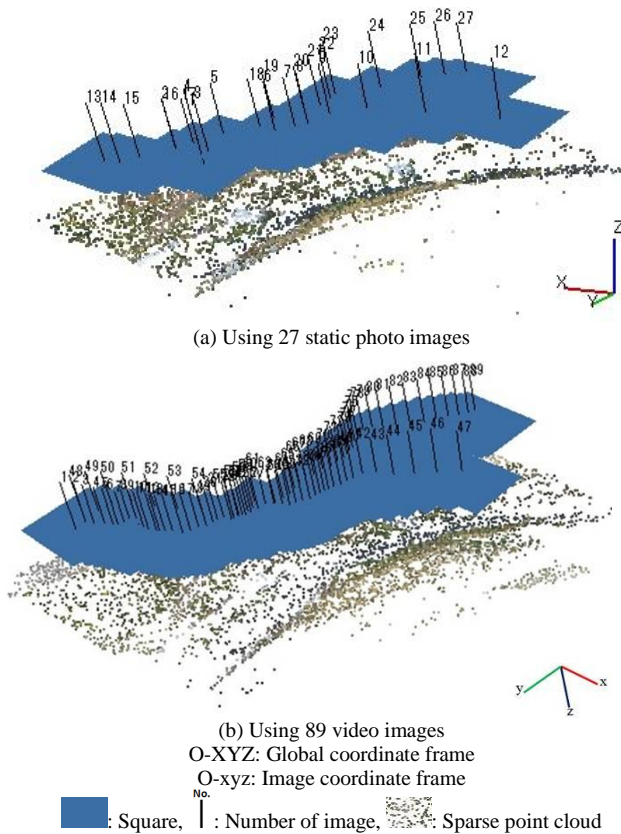


Fig. 9. Estimated positions and orientations of static photo images and video images shown by the squares and the sparse point clouds below the positions displayed in the model plane of the Agisoft

3.3 Building Dense Point Clouds

In the third process, the sparse point clouds and the estimated positions and orientations of the static photo images and the video images were used by the Agisoft to build dense point clouds. There are five quality parameters to build the dense point clouds, namely ultra high, high, medium, low and lowest. The higher the quality becomes, the more complex the resulting dense point clouds will become. Therefore, the dense point clouds were built with the medium quality in order to reduce the complexity of the dense point clouds. In this process, the 749,813 points were generated in the dense point cloud of the static photo images and the 977,575 points in the dense point cloud of the video ones. Figure 10 shows the dense point clouds built from the sparse point clouds and the estimated positions and orientations of the static photo images and video images.

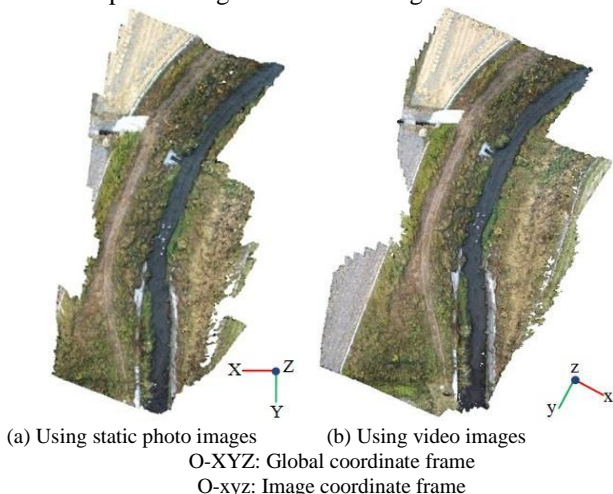
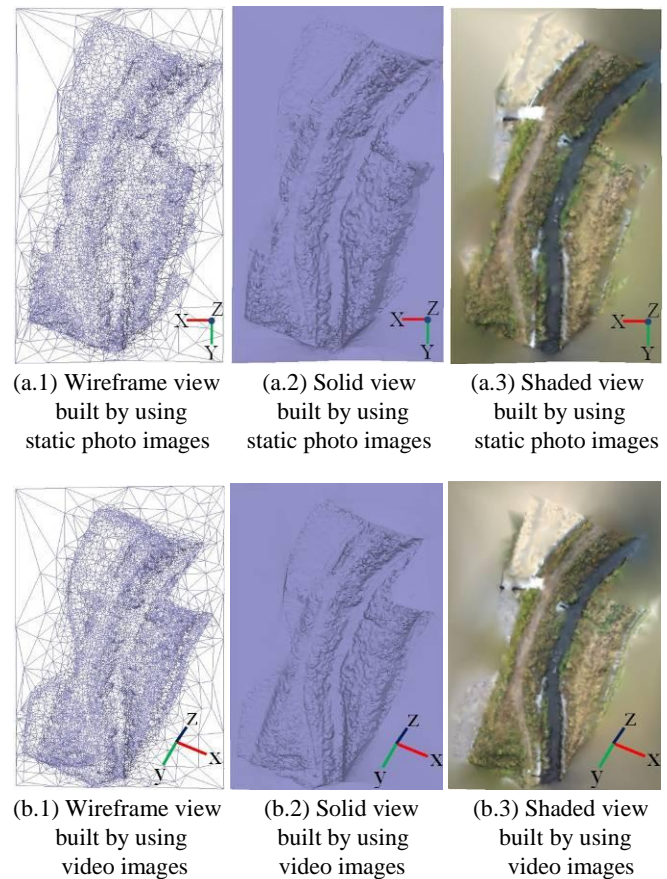


Fig. 10. Dense point clouds built using the sparse point clouds and the estimated positions and orientations of the static photo and video images

3.4 Building Polygonal Meshes

In the fourth process, polygonal meshes were built by using the dense point clouds of the static photo images and video images. There are two types of surfaces on the parameters to build the polygonal meshes, namely the options of “arbitrary” and “height field”. The option of “arbitrary” is used for the surfaces of isolated objects and the option of “height field” is used for the surfaces of terrains. Then, the polygonal meshes were built with the option of “height field”. The polygonal meshes were displayed in three types of views, namely wireframe, solid, and shaded views. In the shaded views, the existing texture data in the dense point clouds of the static photo images and video images were used to texture the solid view of the polygonal meshes. However, some parts in the dense point clouds do not have texture data. Therefore, some parts in the shaded views also do not have texture data. Figure 11 shows the polygonal meshes built by using the dense point clouds of the static photo images and video images.



O-XYZ: Global coordinate frame
O-xyz: Image coordinate frame

Fig. 11. Polygonal meshes built by using the dense point clouds of static photo images and video images

3.5 Building 3D Textured Maps

In the fifth process, 3D textured maps were built by using the shaded views of the polygonal meshes of the static photo images and video images. The texture data of the shaded views of the polygonal meshes were firstly read by the Agisoft. Then, new texture data calculated using the existing ones were generated by the Agisoft for the parts without texture data. Furthermore, 3D textured maps were built by texturing the whole parts of the shaded views using the existing and new texture data. Figure 12 shows the 3D

textured maps showing the geometry and the texture of the environment around the river built using the polygonal meshes of static photo images and video images.

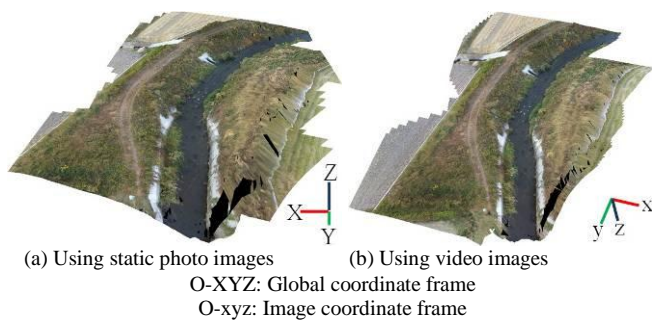


Fig. 12. 3D textured maps showing the geometry and the texture of the environment around the river built using the polygonal meshes of static photo images and video images

The 3D textured maps represent the geometry and the texture of the environment around the river. The lengths and the widths of the maps representing the environment correspond to 27 [m] and 20 [m], respectively for the actual one. It can be seen that the 3D textured map of the static photo images is better than the video ones due to that the average quality of the static photo images is higher than that of the video ones. In addition, the orientation of the 3D textured map of static photo images is more accurate than that of the video ones due to that the static photo images have 3D coordinate data while the video ones do not have 3D coordinate data. Therefore, the 3D textured map of static photo images was used for the 3D map modeling.

4 3D MAP MODELING USING 3D TEXTURED MAP OF STATIC PHOTO IMAGES

In order to obtain better 3D visualization of the environment around the river, a 3D map model was built by using a selected area in the 3D textured map of the static photo images. In this 3D map modeling, the selected area in the 3D textured map was thickened by using the Blender (Ver.2.7.6b) that is an open software of 3D computer graphics. Then, the 3D map model was built using the thickened 3D map. The 3D printing to build the 3D map model was performed by using the IRIS 3D printer.

4.1 Thickening 3D Textured Map

Firstly, a rectangular area was selected in the 3D textured map of the static photo images using a bounding box in the model pane of the Agisoft. Then, a new 3D map was built by using the selected area. After that, the new 3D map was exported to an OBJ file by using the Agisoft PhotoScan software. The OBJ file contains the 3D geometry data of the new 3D map, namely the 3D coordinates of each point in the new 3D map. Both a JPG file containing the texture data of the new 3D map and an MTL file containing the parameters to map the texture data were generated by the Agisoft in order to keep the texture of the new 3D map. Then, the new 3D map in the OBJ file was thickened by using the Blender. The length, the width, and the height of the thickened 3D map are 21.5 [cm], 15.5 [cm], and 3.0 [cm], respectively. The scale ratio of the thickened 3D map to the real environment was 1:126. Figure 13 shows the new 3D map and the thickened 3D map built by using the selected area in the 3D textured map of static photo images of the environment around the river.

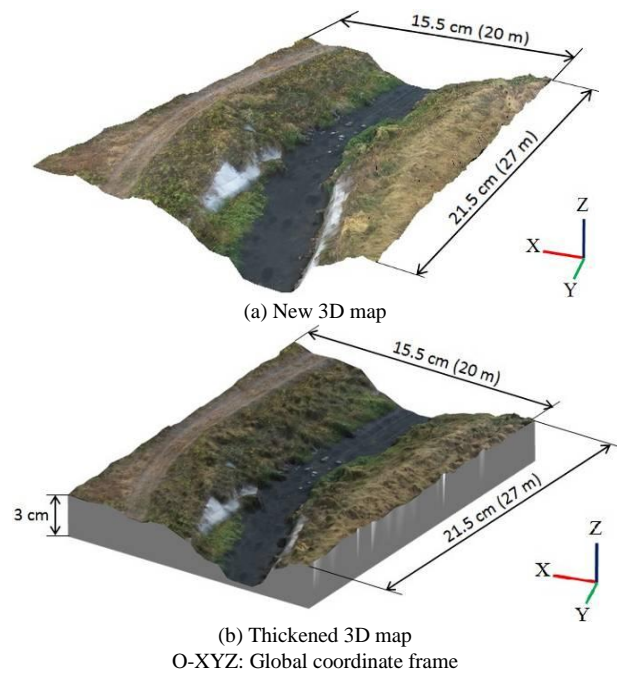


Fig. 13. New 3D map and thickened 3D map (scale ratio of 1:126) built by using the selected area in the 3D textured map of static photo images of the environment around the river

4.2 Preparing Material and Color 3D Printer

A color 3D printer, here the IRIS 3D printer was used to build the 3D map model of the environment around the river. The IRIS 3D printer is connected to a PC installing the SliceIT (Ver.6.1.5) that is the IRIS 3D printer's software. Then, A4 size papers were used as the materials to build the 3D map model. Figure 14 shows both the IRIS 3D printer connected to a PC installing the SliceIT and the A4 size papers prepared to build the 3D map model of the environment around the river.

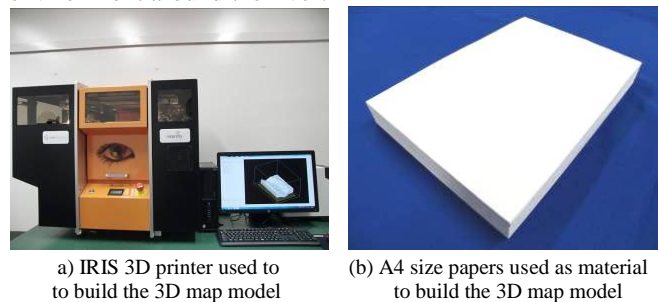


Fig. 14. Both IRIS 3D printer connected to a PC installing the SliceIT and A4 size papers prepared to build the 3D map model

Some processes were performed before starting the 3D printing. Firstly, the thickened 3D map was exported to a new OBJ file by using the Blender software. Both a new JPG file and a new MTL file were also generated by the Blender. Then, those three new files were processed by the SliceIT. The thickened 3D map in the OBJ file was sliced into 337 colored layers by the SliceIT. After that, those layers were printed on 337 pages of A4 size papers by using an ordinary color printer connected to the PC. The colors printed on each page of paper describe the geometry and the texture of each layer of the thickened 3D map. Furthermore, those 337 pages of papers were loaded into the paper tray of the IRIS 3D printer. Both a knife and a bottle of adhesive glue were set inside the IRIS 3D printer to build the 3D map model of the environment around the river using the 337 pages of A4 size papers.

4.3 Printing 3D Map Model

The 3D printing was performed after finishing the preparation of the material and the IRIS 3D printer. Firstly, the first page of papers was pulled from the paper tray and placed on a build plate inside the IRIS 3D printer. Then, the geometry data of the first layer were read by the SliceIT. After that, the commands of both cutting and applying adhesive were generated by the SliceIT based on the geometry data. The commands were sent from the PC to the IRIS 3D printer. The processes of the cutting and applying adhesive were performed by the IRIS 3D printer on the first page of papers. After finishing the processes on the first page, the second page was pulled and placed on the first page. Both pages were pressed by the heat plate inside the IRIS 3D printer. Then, the whole processes were repeated from the second page to the 337th page of papers. After that, the 337 pages of papers containing the 3D map model were taken out from the IRIS 3D printer. Figure 15 shows the 3D map model inside 337 pages of A4 size papers built by using the static photo images of the environment around the river.



Fig. 15. 3D map model inside 337 pages of A4 size papers built by using the static photo images of the environment around the river

4.4 Result

After finishing the 3D printing, all unnecessary parts around the 3D map model were removed from the 3D map model. Figure 16 shows the final 3D map model of the environment around the river built by using the IRIS 3D printer. The dimensions and the scale ratio of the 3D map model were same as those of the thickened 3D map.

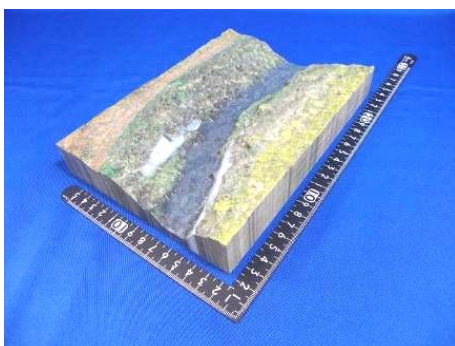


Fig. 16. Final 3D map model of the environment around the river built by using the IRIS 3D printer

5 CONCLUSION

The summary of the results is shown below.

- (1) Firstly, the flying experiment to capture overlapping static photo images and video images of an environment around a river had been performed using the multi-rotor drone with a fisheye-lens camera.

- (2) Then, the image processing of the static photo images and video images to build 3D textured maps had been performed by using the Agisoft PhotoScan. Furthermore, the thickened 3D map was built by using the selected area in the 3D textured map of the static photo images.
- (3) Finally, the 3D map modeling to build a 3D map model of the environment around the river had been performed by using the thickened 3D map. The scale ratio of the 3D map model to the real environment is 1:126.

REFERENCES

- [1] S. Scherer, J. Rehder, S. Achar, H. Cover, A. Chambers, S. Nuske & S. Singh. (2012). River Mapping from a Flying Robot: State Estimation, River Detection, and Obstacle Mapping. *Journal of Autonomous Robots*, Vol. 33 (1-2), pp. 189–214.
- [2] Chambers, S. Achar, S. Nuske, J. Rehder, B. Kitt, L. Chamberlain, J. Haines, S. Scherer & S. Singh. (2011). Perception for a River Mapping Robot. *IEEE/RSJ International Conference on Intelligent Robots and Systems*, pp. 227–234.
- [3] Lari, Z., & El-Sheimy, N. (2015). System Considerations and Challenges in 3D Mapping and Modeling Using Low-Cost UAV Systems. *International Archives of the Photogrammetry, Remote Sensing and Spatial Information Sciences*, vol. XL-3/W3, ISPRS Geospatial Week, 28 Sep – 03 Oct 2015, La Grande Motte, France, pp. 343-348.
- [4] Remondino, F., Barazzetti, L., Nex, F., Scaioni, M., & Sarazzi D. (2011). UAV Photogrammetry for Mapping and 3D Modeling – Current Status and Future Perspectives. *International Archives of the Photogrammetry, Remote Sensing and Spatial Information Sciences*, vol. XXXVIII-1/C22, ISPRS Zurich Workshop, 14-16 September 2011, Zurich, Switzerland, pp. 25-31.
- [5] Barazzetti, L., & Scaioni, M. (2010). Orientation and 3D Modeling from Markerless Terrestrial Images: Combining Accuracy with Automation. *The Photogrammetric Record* 25(132), pp. 356–381.
- [6] Faessler, M., Fontana, F., Forster, C., Mueggler, E., Pizzoli, M., & Scaramuzza, D. (2015). Autonomous, Vision-based Flight and Live Dense 3D Mapping with a Quadrotor Micro Aerial Vehicle. *Journal of Field Robotics* 00(0), pp. 1–20, doi: 10.1002/rob.21581.
- [7] Zongjian, L. (2008). UAV for Mapping—Low Altitude Photogrammetric Survey. *International Archives of the Photogrammetry, Remote Sensing and Spatial Information Sciences*, vol. XXXVII, Part B1, pp. 1183-1186, Beijing.
- [8] Zhang, C. (2008). An UAV-Based Photogrammetric Mapping System for Road Condition Assessment. *International Archives of the Photogrammetry, Remote Sensing and Spatial Information Sciences*, vol. XXXVII, Part B5, pp. 627-631, Beijing.
- [9] Eisenbeiss, H. (2004). A Mini Unmanned Aerial Vehicle (UAV): System Overview and Image Acquisition. *Proceeding of International Workshop on Processing and Visualization Using High-Resolution Imagery*, Pitsanulok, Thailand.
- [10] Covas, J. Ferreira, V. & Mateus, L. (2015). 3D Reconstruction with Fisheye Images: Strategies to Survey Complex Heritage Buildings. *IEEE*. 978-1-5090-0048-7/15.
- [11] Kedzierski, M., & Fryskowska, A. (2009). Application of Digital Camera with Fisheye-lens in Close Range Photogrammetry. *ASPRS 2009 Annual Conference*, Baltimore, Maryland, March.
- [12] Kedzierski M., & Walezykowski P. (2007). Fisheye-lens Camera System Application to Cultural Heritage Data Acquisition. *XXI International CIPA Symposium*, Athens, Greece.
- [13] Bertin, S., Friedrich, H., Delmas, E., & Chan, G. (2014). DEM Quality Assessment with a 3D Printed Gravel Bed Applied to Stereo Photogrammetry. *Photogrammetric Record* 29 (146), pp. 241–264, doi: 10.1111/phor.12061.
- [14] Nakayama, Y., Takewa, Y., Sumikura, H., Yamanami, M., Matsui, Y., Oie, T., Kishimoto Y., Arakawa, M., Ohmura, K., Tajikawa, T., Kanda K., & E. Tatsumi. (2015). In-body tissue-engineered aortic valve (Biovalve type VII) architecture based on 3D printer molding. *Journal of Biomedical Materials Research B: Applied Biomaterials*, vol. 103b, Issue 13, pp. 1–11.
- [15] Olmo, M., Ortega, V., Banos, A., Guirad, C., Regi, V., Arcos, D., & Baeza, A. (2012). In-vivo behavior of Si-hydroxyapatite/ polycaprolactone/DMB scaffolds fabricated by 3D printing. *Journal of Biomed Mater Res, Part A* 2012:00A.
- [16] Metzger, M.C., Majert, B.H., et. al. (2008). Manufacturing splints for orthognathic surgery using a three-dimensional printer. *Oral Surg Oral Med Oral Pathol Oral Radiol Endod*, vol. 105, No. 2, pp. 1-5.
- [17] Taufik A., Okamoto, S., & Lee J.H. (2015). Multi-Rotor Drone to Fly Autonomously Along a River Using a Single-Lens Camera and Image Processing. *International Journal of Mechanical Engineering*, vol. 4, No. 6, pp. 39-49.
- [18] Taufik, A., Okamoto, S., & Lee, J.H. (2015). Multi-rotor Craft with Single-Lens Camera that Can Autonomously Fly along a River. *Proceeding of APCEAS (Asia-Pacific Conference on Engineering and Applied Sciences)*, pp. 195-208, Osaka, Japan.
- [19] Taufik, A., Okamoto, S., & Lee, J.H. (2016). 3D Mapping of an Environment Around a River Using Image Processing of Photo Images Captured by a Multi-Rotor Drone and 3D Modeling Using a 3D Printer. *Proceeding of ECBA (International Conference on Society of Engineering & Technology, Computer, Basic & Applied Sciences)*, vol. 127, Issue 5, pp 1-9, Seoul, South Korea.